EMBEDDABLE LOW-VOLTAGE MICROPUMP USING ELECTROOSMOSIS OF THE SECOND KIND

T. Heldal*, T. Volden*, J. Auerswald**, H. Knapp**,

* IQ Micro Inc, West Palm Beach, FL 33401, USA
trond.heldal@osmotex.no
** Swiss Center for Electronics and Microtechnology (CSEM SA), Alpnach, Switzerland

ABSTRACT

A low-voltage micropump with no moving parts and based on standard MEMS fabrication techniques has been developed. The pump has been characterized by pumping a variety of liquids, including de-ionized water, phosphate buffer saline, and aqueous solutions of sugars and alcohols as well as pure methanol, with typical pumping speeds of a few hundred micrometer per second. The small power/voltage requirements and dimensions make the pump suitable for portable, embedded and implantable devices. The pump is situated inside the flow channel and can therefore be directly integrated in high-density microfluidic networks.

Keywords: micropump, electroosmosis of the second kind, low-voltage, ac, microfabrication

1 INTRODUCTION

Microfluidics is expected to have a great impact on several sciences. Complicated tasks such as DNA analysis, drug-discovery and (bio)chemical research could be automated through lab-chips, extending the capacity in a similar way as the integrated circuit did for computational power. Disposable chips could carry out multiple diagnostic tests, or monitor traces of bio hazard or explosive agents in the air. Yet other applications include micro fuel cells for portable electronics, and implantable insulin pumps for diabetes patients. While sensors and fluidic network can be fabricated on chip level, large grid-powered pumps are usually applied for moving the fluids. Thus, it is recognized that an enabling "microfluidic transistor" technology is needed, i.e. a pump which can be integrated on a chip level [4].

Based on recent findings in electrokinetics, in particular the discovery of electroosmosis of the second kind (EO2) [1], the pump design allows for liquid transport at much lower voltages (usually between 2–50 V depending on application) than what is common in conventional electroosmosis and electrophoresis. The non-linearity of EO2 also enables directed transport using an alternating (AC) field, thereby reducing negative effects associated with DC pumping (such as electrolysis, gas evolution and concentration gradients). It has proven possible to integrate this pump on a chip level, and it can be controlled by standard low-voltage electronics.

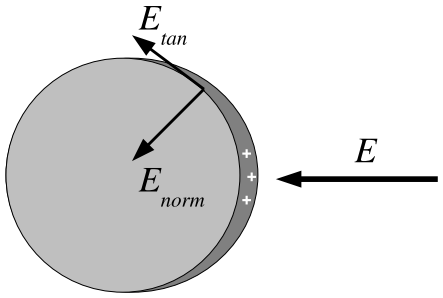

Figure 1: Transport mechanism: The normal electric field component E_{norm} induces a space-charge layer on the ion-exchange element, while the tangential component E_{tan} sets the charges in motion, resulting in EO flow.

2 THEORY

EO2 can be observed at surfaces of unipolar conductors such as ion-exchange polymers, where electric field-induced concentration polarization results in a space-charge layer (see Fig. 1). Using circular geometries, the normal electric field component results in polarization, whilst the tangential component sets the charges in motion. The resulting EO flow is 1–2 orders of magnitude larger than for classical electroosmosis, for a given electric field strength. Other non-linear effects known as "AC electrokinetics" and "induced-charge electroosmosis" [2] are significantly weaker.

Classical (linear) electroosmosis is governed by the Smoluchowsky equation (1):

$$v_{eo1} = \frac{\varepsilon \zeta E}{\eta} \tag{1}$$

Here, v_{eo1} is the liquid velocity, ε the liquid permittivity, ζ the zeta potential characterizing the electric double layer (EDL), E the electric field strength and η the liquid viscosity. This phenomenon is frequently studied in cylindrical capillaries, where a plug flow results from electroosmosis originating on the pore walls.

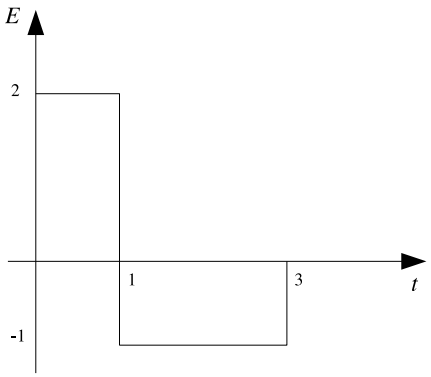

Figure 2: Electric AC signal with offset and duty-cycle.

For electroosmosis of the second kind, the dependencies on both normal and tangential field strength components results in a proportionality between EO flow velocity and the squared electric field strength (2):

$$v_{eo2} = \frac{\varepsilon E^2 a}{\eta} \tag{2}$$

Here, a is the particle radius. The nonlinear dependency on the driving voltage seen in equation 2 allows for directed pumping using an asymmetric AC signal with zero DC component (figure 2).

For pumps, not only the flow velocity, but also the achievable pressure is of importance. Laminar pressure-driven flow in porous media can be modeled by the Hagen-Poiseuille equation, which can be written for a single pore:

$$v_{\nabla p} = \frac{r^2 \Delta p}{8 \Delta x \eta} \tag{3}$$

Here ∇p is the pressure gradient, Δx the dimension of the porous material parallel to the pressure drop, and r the pore radius. Combining equations 2 and 3 yields the following relation for the EO2 pressure:

$$\Delta p^{EO2} = \frac{8 \varepsilon E^2 \Delta x a}{r^2} \tag{4}$$

This shows that reducing the pore size by a factor of 10 leads to a 100-fold increase in pressure.

3 EXPERIMENTAL

The pump components are all fabricated inside the flow channel, resulting in a highly compact pumping device (see Fig. 3). The depicted pump consists of forty polarizable beads (i.e. active elements) with a diameter of approximately 100 μm, placed in a channel with a height of 90 μm and a width of 800 μm (part of the active elements going into the channel ceiling). The driving electrodes, made out of deposited gold structures, are also placed inside the channel, with a spacing of 1200 μm.

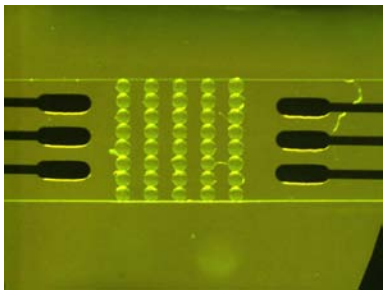

Figure 3: Micrograph showing the pump section of a 40-element system with beads of 100-μm diameter. The effective pore diameter of the active section is 30 μm, and the electrode spacing is 1200 μm.

Quantitative tests were carried out using a metal and transparent polymer packaging, with either zero-counter-pressure or zero-flow conditions, a setup for the latter is shown in figure 4. DC signals as well as asymmetric AC signals (see Fig. 2) were applied in these tests, and DI water was used as fluid medium.

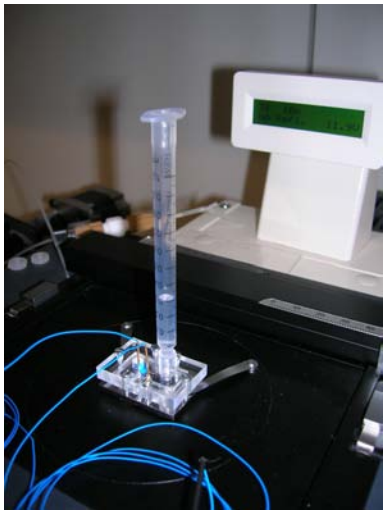

Figure 4: Pump system with water column for applying counter-pressure.

A number of tests were carried out using different embodiments of the EO2 micropump (differing in size and number of active elements, channel dimensions and electrode distances). Successful pumping was demonstrated for liquids used in bio-sciences (phosphate buffer saline, mannitol), fuel for fuel-cells (pure methanol and aqueous solutions), and coolants (ethylene glycol solutions). Since the counter pressure was not controlled, these tests should be regarded as qualitative.

The smallest pump consisted of three polarizable sPS-DVB beads with a diameter of 50 μm, placed inside a channel with a height of 50 μm and a width of 180 μm (figure 5). The electrode spacing was here 750 μm, and the maximum channel length was 15 mm. A third pro-

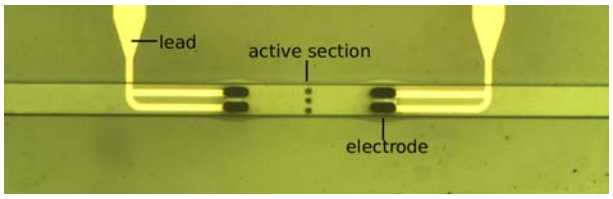

Figure 5: Micrograph showing the pump section of a 3-element system with beads of 50-μm diameter. The electrode spacing is 750 μm.

totype uses six molded 200-μm cylinders (height 50 μm) of sulfonated polyether-ether-ketone (PEEK). Pumping performance was measured using fluorescent dyes or microbeads for flow visualization.

4 RESULTS AND DISCUSSION

4.1 40-Element System

Results from AC tests are shown in figure 6. The two curves show pumping in either direction, controlled by selecting the polarity of the strong pulse of the signal in figure 2. The resulting directed flow confirms the non-linear relation between flow and electric field strength. For simpler comparison with the main equations, the rest of the experiments were carried out using DC driving voltages, eliminating various time-dependent effects.

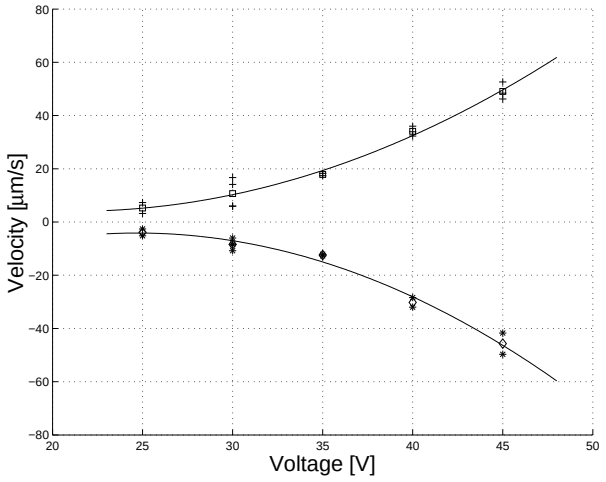

Figure 6: Experimental flow rates using AC voltage, pump with forty 100-μm beads (loop system).

Theoretical and experimental flow rates for a closed-loop system are presented in figure 7, while maximum pumping pressure is presented in figure 8. The channel cross-section is 800 μm times 90 μm. While there is clearly a non-linear flow-voltage relationship, the velocity is lower than the predicted value. One explanation could be the large effective pore size of 30 μm, making the pump very sensitive to any channel flow resistance, due to the low pumping pressure. Another reason could be the creation of turbulence in addition to directed flow, which was observed by flow visualization using small particles. This is also not surprising when using spherical active elements, for this reason more optimized shapes are under investigation. Another reducing factor might be the feeding of ions into the charged zone of a bead in one row from the opposite (concentrated) side of a bead in the adjacent row. This might also be a reason for the discrepancy between experimental and calculated pressure, however in this case the values are in better agreement. Channel flow resistance will not affect these measurements, as they are taken under zero-flow conditions.

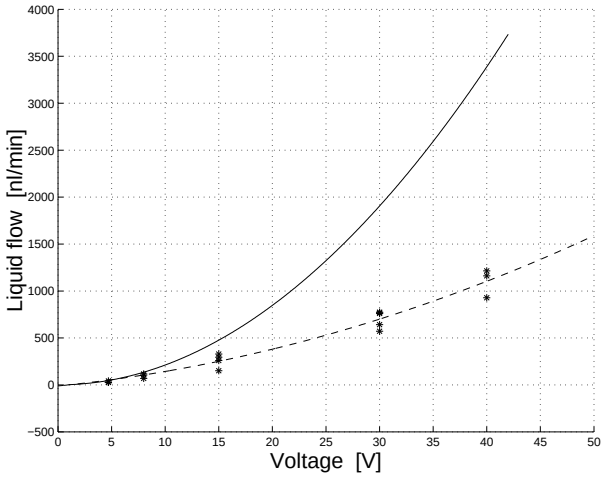

Figure 7: Calculated (solid line) and experimental (dashed line) flow rate, 40-element pump, closed loop.

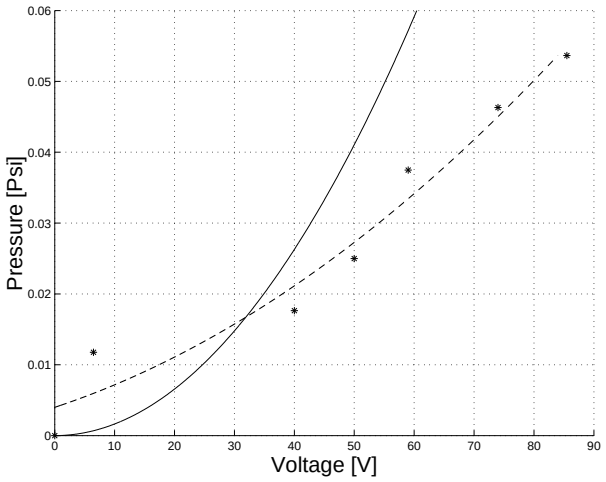

Figure 8: Calculated (solid line) and experimental (dashed line) EO2 pressure, 40-element pump, at zero flow.

As can be seen from figure 9, the experimental data

NSTI-Nanotech 2007, www.nsti.org, ISBN 1420061844 Vol. 3, 2007

Table 1: Pump performance using liquids for life sciences, fuel cells and liquid cooling applications. The tests were performed in an open system. Using an AC square-pulse signal with offset and duty-cycle.

Liquids	Electric signals	Flow velocities
DI water ethylene glycol(aq) 36/52% mannitol 280 mM PBS 0.02/0.2/2mM $[Na^+]$	5–10 VDC 15–30 VAC (1–30Hz)	0.01–2 mm/s (approx. 0.1–20 nl/s)

are in accordance with the calculated value for 10^{-4} M NaCl concentration. The DI water was measured to have 10^{-5} M ionic concentration before the tests. However, the concentration could have been increased due to water splitting when pumping using DC voltage. No significant difference in power consumption was observed between closed-loop and zero-flow set-up.

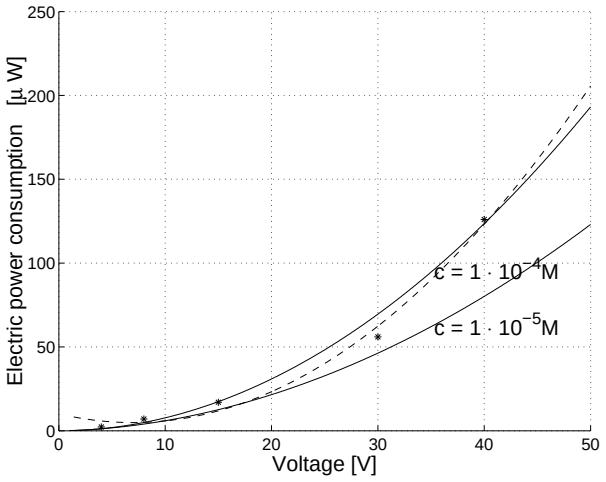

Figure 9: Calculated (solid line) and experimental (dashed line) power consumption, 40-element pump, closed loop. The calculated values are given for two NaCl concentrations.

Currently, higher-pressure pumps are being developed, by optimizing the shape and configuration of the active elements while reducing the pore size, defined by the spacing between the elements. The technology is highly scalable, with the maximum pressure and flow rate being determined by the pore size and the area of the active section, respectively. Furthermore, the maximum frequency of the driving electric signal is determined by the size of the active elements [1].

4.2 Qualitative Tests with Various Liquids

Results from quantitative tests using the 3-active-element system are presented in table 1. In addition, pure methanol was successfully pumped using the 40-active-element system. The results confirm the ability of the devices to pump liquids for a wide range of applications. This is in accordance with theory, which predicts that polar liquids with low to moderate conductivity can be pumped.

5 CONCLUSIONS

Micropumps based on strong polarization electroosmosis have been fabricated and demonstrated to pump a range of liquids using low AC or DC voltages. A power consumption in the microwatt range was demonstrated, as well as a non-linear relationship between driving voltage and flow/pressure. The microfabricated compact design is suitable for integration with microfluidic systems.

The technology is highly scalable, and devices can be designed to yield higher flow rates and pressures.

6 ACKNOWLEDGEMENTS

The authors would like to thank Professor Nataliya Mishchuk at the National Academy of Sciences of Ukraine for many helpful discussions.

REFERENCES

[1] N.A. Mishchuk, P.V. Takhistov, Colloids and Surfaces A 95, pp. 119–131 (1995).

[2] T.M. Squires, M.Z. Bazant, J.Fluid. Mech. 509, pp. 217–252 (2004).

[3] T. Heldal, T. Volden, J. Auerswald, H. Knapp, Proceedings of the MicroTAS Conference 2006, Tokyo, November 5.–9. 2006, pp. 1061–1063.

[4] Business Communication Company, "Microfluidics Technology (SMC036C)", November 2006.